THE JOURNAL OF PHYSICAL CHEMISTRY LETTERS
A JOURNAL OF THE AMERICAN CHEMICAL SOCIETY

pubs.acs.org/JPCL Letter

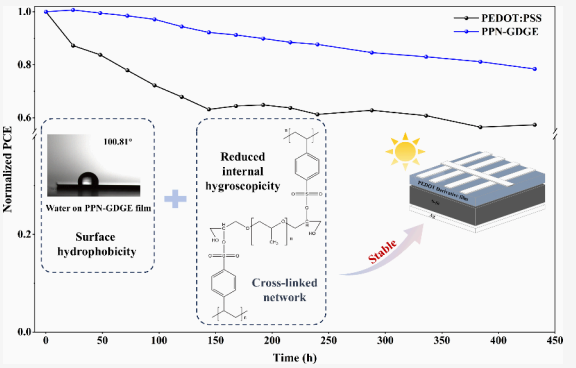
Design of PEDOT Derivative Films with Reduced Hygroscopicity by Dual-Sulfonated Polymer for Stable Si Hybrid Solar Cells

Qi Geng, Wangbo Liu, Yuzhou Liu, Zhe Wang, Zhongliang Gao, Xin Sun, Yingfeng Li, Xiaojun Lv, and Meicheng Li*

Cite This: J. Phys. Chem. Lett. 2026, 17, 5880−5888 Read Online

ACCESS | Metrics & More | Article Recommendations | Supporting Information

ABSTRACT: Poly(3,4-ethylenedioxythiophene):poly(styrenesulfonate) (PEDOT:PSS) is commonly used in optoelectronic devices, but its intrinsic hygroscopicity impairs device stability. Here, a PEDOT derivative film with surface hydrophobicity and reduced internal hygroscopicity was designed through dual-sulfonated polymer, successfully improving the stability of Si hybrid solar cells. The surface hydrophobicity of the film was associated with EG-induced enhanced exposure of the fluorocarbon chains of Nafion, achieving a water contact angle of 108.1°. Furthermore, after poly(propylene glycol) diglycidyl ether (PPGDGE) was introduced to construct a cross-linked network, the internal hygroscopicity of the film was further reduced. As a result, the device retained 78% of its initial power conversion efficiency (PCE) after 432 h of storage in air, compared with only 57% for PEDOT:PSS. This provides a feasible design concept for mitigating the adverse impact of PEDOT:PSS on device stability and also indicates the potential of this film to construct other stable optoelectronic devices.



Downloaded via XIANGTAN UNIV on May 25, 2026 at 04:29:15 (UTC).
See https://pubs.acs.org/sharingguidelines for options on how to legitimately share published articles.

Poly(3,4-ethylenedioxythiophene):poly(styrenesulfonate) (PEDOT:PSS), owing to its good film-forming ability, relatively high conductivity, and solution processability, has been widely used for fabricating high-performance optoelectronic devices.[1−3] In Si hybrid solar cells, PEDOT:PSS not only forms a heterojunction with n-Si but also serves as a hole transport layer and therefore plays an important role in achieving high device performance.[4−10] However, PEDOT:PSS is typically used as the front surface functional layer and is directly exposed to air; therefore, its intrinsic hygroscopicity is detrimental to the long-term stability of devices.[11,12]

In order to improve the stability of Si hybrid solar cells, various strategies have been developed. For example, in terms of additive engineering, hydrophobic molecules or functional additives have been introduced to improve the hydrophobicity of the PEDOT:PSS film and thereby enhance the stability of PEDOT:PSS/Si hybrid solar cells.[13,14] In terms of surface protection of the PEDOT:PSS film, capping layers can effectively block the penetration of moisture, thus improving the stability of PEDOT:PSS/Si hybrid solar cells.[15−17] In addition, weakening the hygroscopicity of the PEDOT:PSS film also provides a route to improve the stability of PEDOT:PSS/Si hybrid solar cells.[18] The above strategies have all played a positive role in improving the stability of Si hybrid solar cells, but most of these methods focus on single pathways such as surface hydrophobic regulation, external physical protection, or weakening the hygroscopicity of the film. Therefore, it remains of great significance to develop a design concept starting from the material itself to construct films with surface hydrophobicity and reduced internal hygroscopicity for improving the stability of Si hybrid solar cells.

In this work, based on the dual-sulfonated polymer PSS and Nafion, we designed a PEDOT derivative film with surface hydrophobicity and reduced internal hygroscopicity for improving the stability of Si hybrid solar cells. By designing the contact sequence among EDOT, PSS, and Nafion, we regulated the film conductivity and identified the optimal sequence for achieving the highest electric conductivity of the films. The surface hydrophobicity of the film originated from the ethylene glycol (EG)-induced redistribution of surface components. Furthermore, the introduction of poly(propylene glycol) diglycidyl ether (PPGDGE) restrained the internal hygroscopic behavior of the film, which was attributed to the formation of a cross-linked network with sulfonic acid groups. On the basis of this film, PEDOT derivative/Si hybrid solar cells were fabricated, exhibiting improved storage stability.

Received: March 26, 2026
Revised: April 22, 2026
Accepted: May 4, 2026
Published: May 7, 2026



ACS Publications © 2026 American Chemical Society

https://doi.org/10.1021/acs.jpclett.6c00980
J. Phys. Chem. Lett. 2026, 17, 5880−5888

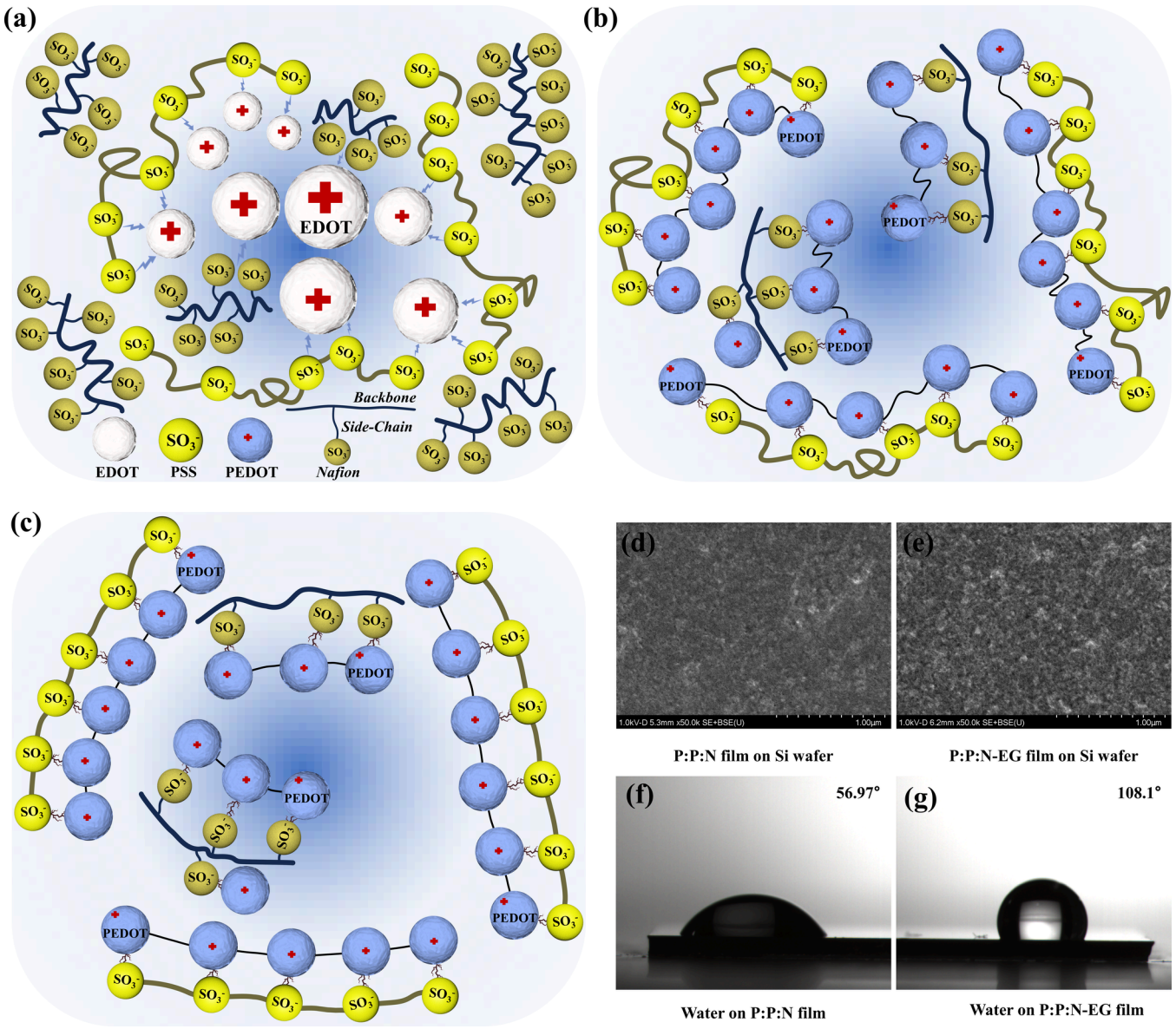


Figure 1. Structural evolution in PPN with corresponding film surface morphology and wettability. (a) Schematic illustration of the preassembly structure of EDOT, PSS, and Nafion before oxidative polymerization. (b) Schematic illustration of the PPN structure after oxidative polymerization. (c) Schematic illustration of the PPN structure after EG addition. Surface SEM images of (d) PPN and (e) PPN-EG films on Si substrates. The contact angles of water on (f) PPN and (g) PPN-EG films.

After 432 h of storage, the best-performing device retained 78% of its initial power conversion efficiency (PCE), significantly higher than the 57% retained by PEDOT:PSS devices.

To mitigate the adverse influence of the intrinsic hygroscopicity of conventional PEDOT:PSS films on the stability of Si hybrid solar cells, we sought to design a PEDOT derivative film with surface hydrophobicity and reduced internal hygroscopicity. On the basis of this idea, PSS and Nafion were introduced into the oxidative polymerization process of EDOT. As shown in Figure S1a, EDOT was first brought into contact with PSS, followed by the introduction of Nafion and subsequent oxidative polymerization to form PPN. Figure S1b–d further shows the dialysis purification, centrifugation, and dispersion processes used to obtain a uniform and stable PPN solution. The other two contact sequences were defined as follows: EDOT was first brought into contact with Nafion, followed by the introduction of PSS (PNP); and EDOT, PSS, and Nafion were brought into contact simultaneously (PPP). Detailed preparation procedures are provided in the Experimental Section of the Supporting Information. Except for the different contact sequences of EDOT with PSS and Nafion, PNP and PPP underwent the same post-treatment procedures as PPN.

To verify the successful polymerization of the PEDOT derivative, the XPS spectra of PPN and PEDOT:PSS films were analyzed, and the elemental compositions of the two films were further compared, as shown in Figure S2. The survey spectrum of the PPN film exhibits S, C, O, and F signals, whereas only S, C, and O are detected in the PEDOT:PSS film in Figure S2a. At the same time, in the C 1s region, the PPN film shows an additional peak at 291.8 eV, which is assigned to the fluorocarbon (C–F) bond of Nafion,[19] while no corresponding high binding energy peak is observed for

https://doi.org/10.1021/acs.jpclett.6c00980
J. Phys. Chem. Lett. 2026, 17, 5880–5888

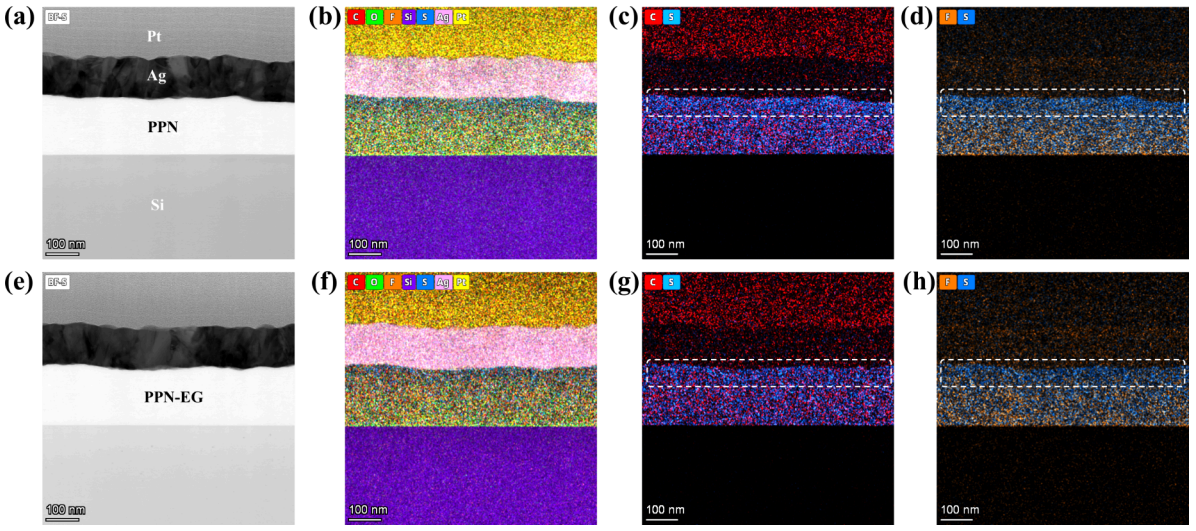


Figure 2. Cross-sectional TEM images and EDS elemental mapping of PPN and PPN-EG films. (a) Cross-sectional TEM image of PPN film. (b) EDS elemental mapping of C, O, F, and S in PPN film. (c) C−S overlay mapping image of PPN film. (d) F−S overlay mapping image of PPN film. (e) Cross-sectional TEM image of PPN-EG film. (f) EDS elemental mapping of C, O, F, and S in PPN-EG film. (g) C−S overlay mapping image of PPN-EG film. (h) F−S overlay mapping image of PPN-EG film.

PEDOT:PSS. In Figure S2b, the PPN film exhibits the characteristic S 2p doublet peaks of PEDOT, confirming the successful formation of the PEDOT structure.[20] The peak at 168.5 eV is attributed to sulfonic acid groups, and the double peaks between 164 and 165 eV correspond to PEDOT. Notably, the S 2p peak of PPN shifts slightly toward a higher binding energy relative to that of PEDOT:PSS. This may be associated with the introduction of Nafion during polymerization because the strong electron-withdrawing character of fluorocarbon chains in Nafion reduces the electron density around the sulfonic acid groups.[19] In addition, a distinct F signal at 688.9 eV is observed for the PPN film but is absent in PEDOT:PSS, as shown in Figure S2c. These results confirm the successful incorporation of Nafion into the polymer framework and the construction of PPN. Next, the electric conductivity of the films prepared under the three different contact sequences was further evaluated. The electric conductivity was calculated according to eq 1:

$$\sigma = \frac{1}{\rho \times A \times \mathrm{h}} \tag{1}$$

The detailed measurement method has been reported in our previous work,[21] where ρ represents the resistance per unit width of the film, A is the length of the Ag grid electrode (1.7 cm), and h is the film thickness. It was found that the electric conductivity strongly depends on the contact sequence in Figure S2d. The PPN film exhibits the highest electric conductivity of 36.51 S/cm, followed by PNP (31.41 S/cm), whereas PPP shows the lowest value of 24.07 S/cm. As shown in Figure S2e, the three kinds of films have nearly identical thicknesses of about 494 nm, indicating that the effect of thickness on the electric conductivity calculation can be neglected. The corresponding ρ values and extraction process are shown in Figure S3.

The schematic microstructural models of PPN at different processing stages are proposed in Figure 1. A localized preassembled state can form when EDOT is first brought into contact with PSS before oxidation, as shown in Figure 1a. EDOT can be protonated under acidic conditions.[22] Because the sulfonic acid groups on the PSS chains are negatively charged, the preferential contact between EDOT and PSS is conducive to the formation of localized preassembled structures through electrostatic interactions, causing EDOT to be preferentially distributed around the PSS chains in a relatively uniform manner. After Nafion is introduced, its sulfonic acid groups can further interact with EDOT monomers that have not been fully associated in the system. However, because the preassembled structure of EDOT and PSS has already formed, the spatial distribution of Nafion may be affected, resulting in a state in which part of Nafion is associated with EDOT while the rest remains relatively free. The structural state after oxidative polymerization and subsequent dispersion into solution is illustrated in Figure 1b. Under the effect of oxidation, EDOT monomers are polymerized into positively charged PEDOT, while the sulfonic acid groups in the system serve as counterions to maintain charge balance. Because localized preassembled structures have already formed at the precursor stage, they can be partially retained during polymerization, causing PEDOT to preferentially grow around the PSS chains and form PEDOT:PSS structures. Meanwhile, EDOT previously interacted with Nafion can also be polymerized into PEDOT:Nafion structures. Their spatial distribution may partially interpenetrate with that of PEDOT:PSS rather than forming completely isolated regions. Considering that EG is known to induce a conformational rearrangement of PEDOT chains and influence the local distribution of conductive domains in PEDOT:PSS,[23] EG was further introduced. As illustrated in Figure 1c, the PEDOT chains may evolve from relatively coiled conformations to more extended ones under the EG-induced effect. This conformational change is favorable for the formation of conductive domains on the local scale. The corresponding surface morphologies of PPN films are also shown in Figure 1d,e. The film without EG is smooth and compact, whereas the EG-treated film is slightly rougher, which may lead to the change in surface hydrophobicity. Figure 1f,g shows the water contact angles on the film surfaces. The PPN film without EG exhibits a water contact angle of 56.97°, indicating a hydrophilic surface, whereas the EG-treated PPN

https://doi.org/10.1021/acs.jpclett.6c00980
J. Phys. Chem. Lett. 2026, 17, 5880−5888

Table 1. Electrical Output Parameters of Si Hybrid Solar Cells Constructed with Different Films before and after 432 h[a]

	J_{SC} (mA/cm^2)	V_{OC} (V)	FF (%)	PCE (%)
PPN/Si	22.5 (22.26 ± 0.63)	0.564 (0.556 ± 0.006)	59.13 (60.54 ± 2.42)	7.51 (7.49 ± 0.1)
PPN-GDGE/Si	23.26 (22.87 ± 0.25)	0.562 (0.559 ± 0.002)	58.01 (58.6 ± 0.56)	7.59 (7.5 ± 0.09)
PEDOT:PSS/Si	30.27 (30.52 ± 0.31)	0.560 (0.560 ± 0.002)	69.37 (69.83 ± 0.49)	11.76 (11.94 ± 0.15)
PPN/Si-432 h	21.8 (21.39 ± 0.48)	0.555 (0.552 ± 0.002)	39 (40.76 ± 1.76)	4.72 (4.82 ± 0.26)
PPN-GDGE/Si-432 h	23.11 (22.74 ± 0.21)	0.548 (0.546 ± 0.003)	46.96 (46.53 ± 0.55)	5.95 (5.78 ± 0.11)
PEDOT:PSS/Si-432 h	30.29 (30.22 ± 0.36)	0.520 (0.521 ± 0.001)	42.78 (44.52 ± 1.35)	6.74 (7.02 ± 0.22)

[a]The data in parentheses were calculated from five sets of solar cells.

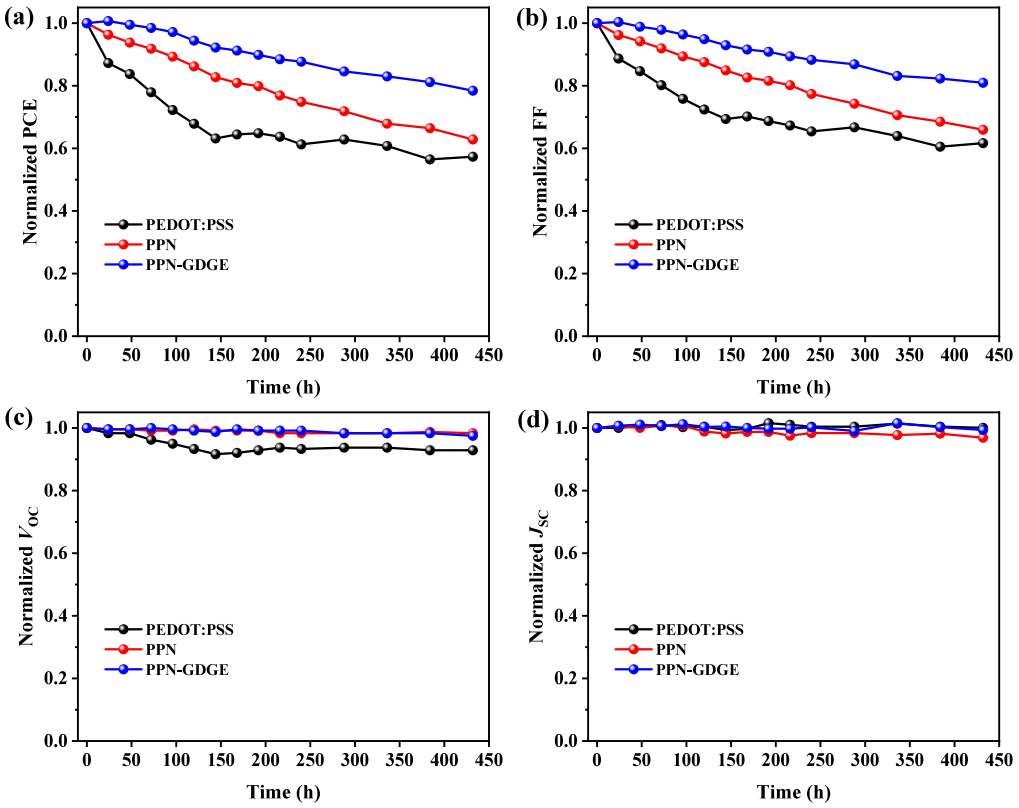


Figure 3. Normalized photovoltaic parameters of different Si hybrid solar cells over time: (a) PCE, (b) FF, (c) V_{OC}, and (d) J_{SC}.

film shows a contact angle of 108.1°, demonstrating obviously surface hydrophobicity. This behavior is likely related to the EG-induced structural rearrangement in the film. Specifically, EG may promote phase separation of PEDOT and PSS and drive the C−F chains of Nafion to become more exposed at the film surface. Therefore, the film exhibits good surface hydrophobicity.

As shown in Figure S4a, the case in which EDOT preferentially contacted with Nafion was similar to PPN, but Nafion has different structures in pure water and alcohol/water mixed solvents.[24−26] Under the alcohol/water condition used in this work (the volume ratio was 6:1), the exposure of Nafion side chains is reduced, while the C−F backbone becomes more pronounced before and after EG addition in Figure S4b,c. This structural change may affect the local formation of conductive domains, which may account for the lower conductivity of the PNP film compared with that of PPN. In addition, the surface morphology of the PNP film is nearly identical to that of PPN in Figure S4d,e, while its water contact angle increases from 58.66° without EG to 105.94° after EG introduction in Figure S4f,g. This indicates that EG can also enhance the surface hydrophobicity of the PNP film and further supports the judgment that EG induces changes in the surface exposure of film components. As shown in Figure S5a−c, when EDOT, PSS, and Nafion are brought into contact simultaneously, EDOT may interact with the sulfonic acid groups of both polymers at the same time, triggering competitive effects. As a result, it is difficult to form localized preassembled structures dominated by a single component, even after the introduction of EG. Notably, the PPP film exhibits obvious large particle aggregation and poor film quality, together with the lowest conductivity, as shown in Figure S5d,e. Meanwhile, its water contact angle increases from 67.13° to 108.65° after EG introduction in Figure S5f,g. Although none of the three pristine films exhibited hydrophobicity, their water contact angles were still higher than that of 17.04° of the PEDOT:PSS film in Figure S6.

To demonstrate the inducing effect of EG on the surface components of thin films, the cross-sectional TEM images of the PPN and PPN-EG films are shown in Figure 2a,e. From top to bottom, the layers correspond to the Pt, Ag protective layer, PPN or PPN-EG film, and Si substrate. The corresponding elemental distributions obtained from energy-dispersive X-ray spectroscopy (EDS) clearly show the spatial

https://doi.org/10.1021/acs.jpclett.6c00980
J. Phys. Chem. Lett. 2026, 17, 5880−5888

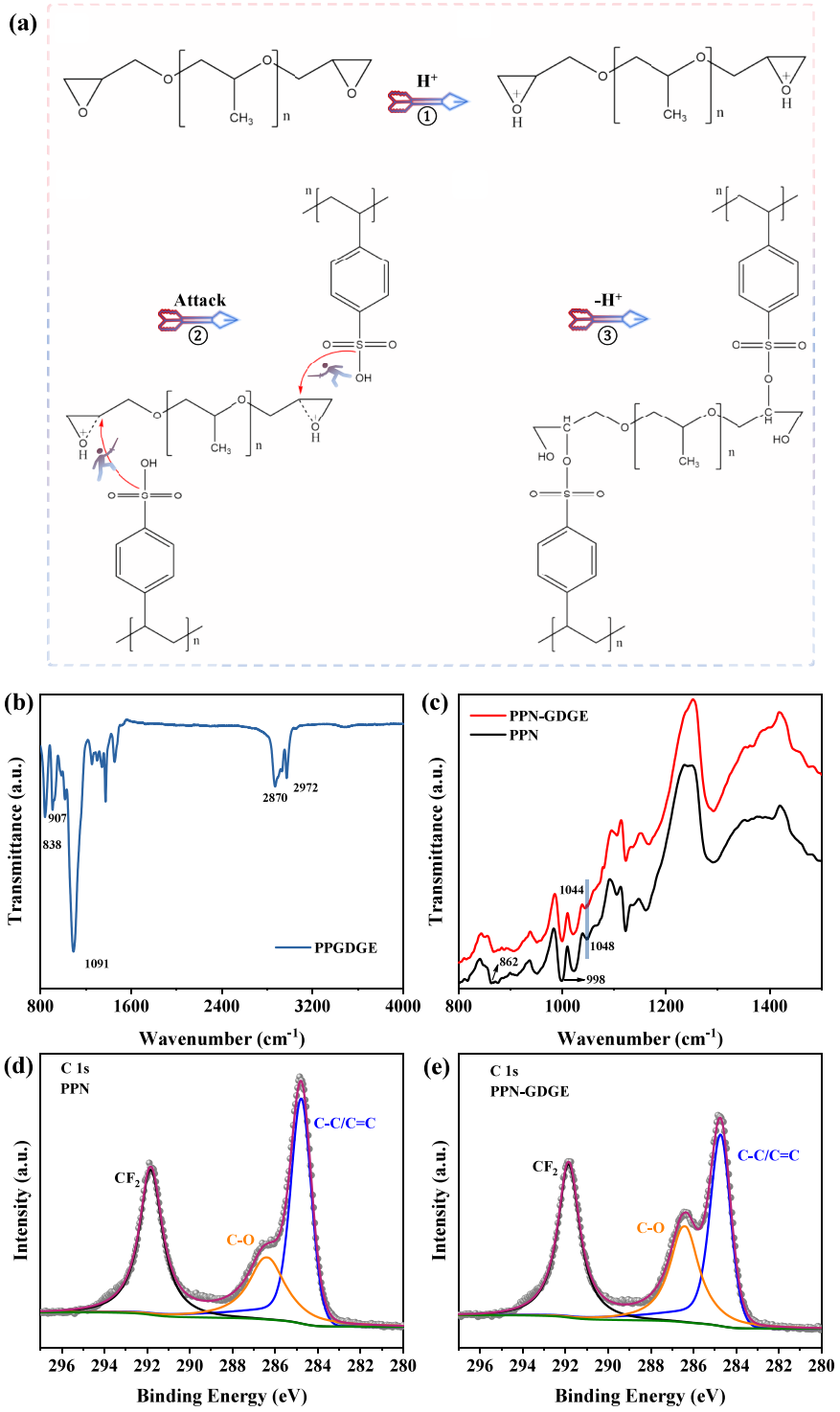


Figure 4. The reaction pathway of PPGDGE in the PPN solution and verification. (a) The reaction pathway of PPGDGE in the PPN solution. (b) FTIR spectrum of PPGDGE. (c) FTIR spectra of PPN and PPN-GDGE films. XPS spectra of C 1s core level of (d) PPN and (e) PPN-GDGE films.

distributions of C, O, F, and S within the PPN and PPN-EG films in Figure 2b,f. Overall, the surface distribution of S is obvious in the PPN film, whereas the surface distributions of C and F become more obvious in the PPN-EG film. To further compare the surface distribution characteristics of different elements, we compared the overlay images of C−S and F−S elements. In Figure 2c, the overlay image of C−S of the PPN film shows a more obvious surface distribution of S, whereas the distribution of C appears to be largely masked by the S distribution. In contrast, the surface distribution of C becomes more obvious in the PPN-EG film, as shown in Figure 2g. Considering that Nafion contains hydrophobic C−F chains, the surface distributions of C and F are expected to exhibit similar variation trends. This is also supported by the overlay image of F−S. As shown in Figure 2d, the surface distribution of S is more obvious in the PPN film, whereas the surface

https://doi.org/10.1021/acs.jpclett.6c00980
J. Phys. Chem. Lett. 2026, 17, 5880−5888

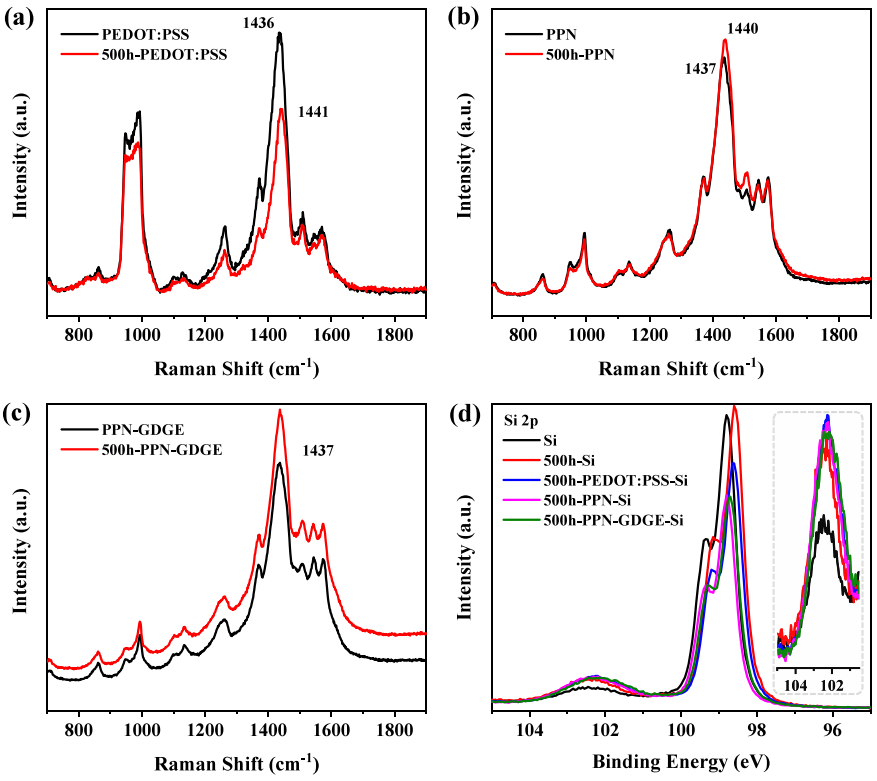


Figure 5. Raman spectra of different films and XPS spectra of the corresponding Si surface. (a) Raman spectra of pristine PEDOT:PSS film and the film stored in air after 500 h. (b) Raman spectra of pristine PPN film and the film stored in air after 500 h. (c) Raman spectra of pristine PPN-GDGE film and the film stored in air after 500 h. (d) Si 2p core level spectra of HF-etched Si, Si, and the Si surfaces after the removal of PEDOT:PSS, PPN, and PPN-GDGE films.

distribution of F appears to be largely masked by the S distribution. In contrast, in the PPN-EG film shown in Figure 2h, the surface distribution of F becomes more obvious. These results indicate that EG induces the redistribution of surface components and promotes the exposure of the hydrophobic C−F chains of Nafion at the film surface. This endows the PEDOT derivative film with surface hydrophobicity.

Based on the above analysis of the electric conductivity and surface hydrophobicity of the three kinds of films, we used PPN, PNP, and PPP films to construct Si hybrid solar cells directly and further investigated their influence on device performance. The current density−voltage ($J-V$) curves of the three kinds of Si hybrid solar cells are shown in Figure S7, and the detailed electrical output parameters are shown in Table S1. Among the three devices, the PPN/Si hybrid solar cell exhibits the best photovoltaic performance, with a PCE of 7.51%. In comparison, the PCE of the PNP/Si device was 7.1% due to the decrease of the fill factor (FF). The PCE of the PPP/Si device was 6.1% because of the poorer surface morphology and lower electric conductivity of the PPP film.

Furthermore, the storage stability of the PPN/Si hybrid solar cell with the highest PCE among the three devices and the PEDOT:PSS/Si hybrid solar cell was evaluated in air at a relative humidity of 20%−30%. The detailed electrical output parameters are shown in Table 1, and the four normalized photovoltaic parameters of the devices are shown in Figure 3. Under the same testing conditions, the PCE of the PEDOT:PSS device decreased more noticeably within 150 h, whereas the PCE of the PPN device decreased more slowly. After 432 h of storage, the PPN device still retained 62% of its initial PCE, decreasing from 7.51% to 4.72%, while the PEDOT:PSS device retained only 57%, with its PCE decreasing from 11.76% to 6.74%, as shown in Figure 3a and Table 1. This difference is mainly attributed to the stronger surface hydrophobicity of the PPN film. In Figure 3b, the decay trend of FF was generally consistent with the trend of the PCE of PPN/Si and PEDOT:PSS/Si hybrid solar cells. We also found that the open-circuit voltage (V_{OC}) of the PEDOT:PSS device decreased during the early stage, but that of the PPN device remained relatively stable, as shown in Figure 3c. Meanwhile, the short-circuit current density (J_{SC}) of both devices remained nearly unchanged throughout the entire testing period, as shown in Figure 3d.

Overall, although the PPN device exhibits better stability than the PEDOT:PSS device, the extent of improvement is still limited. This indicates that, although the surface hydrophobicity of the film can improve the stability of the device, the internal hygroscopicity of PSS within the film bulk still has a negative impact on the long-term stability of the device. Therefore, PPN was further modified with poly(propylene glycol) diglycidyl ether (PPGDGE) to reduce the internal hygroscopicity of the film and improve the stability of PPN/Si hybrid solar cells. As shown in Figure 3a, the decrease in PCE of the PPN-GDGE device was clearly slowed over the entire testing period compared to that of PPN. After 432 h, the device still retained 78% of its initial PCE, decreasing from 7.59% to 5.95%. Meanwhile, as shown in Figure 3b, FF exhibited a similarly slow decline trend as PCE, while the V_{OC} and J_{SC} remained stable throughout the entire testing period, as shown in Figure 3c,d. On this basis, the performance of the PPN-GDGE/Si hybrid solar cell was further evaluated. The $J-V$ curve and detailed electrical output parameters are shown in

https://doi.org/10.1021/acs.jpclett.6c00980
J. Phys. Chem. Lett. 2026, 17, 5880−5888

Figure S8a and Table 1. The results indicate that the introduction of PPGDGE does not cause a negative effect on the device PCE compared with the PPN device. Meanwhile, the PPN-GDGE device still maintains a relatively stable EQE response, as shown in Figure S8b. Although its PCE is lower than that of the PEDOT:PSS device in Figure S8, it exhibits better stability.

To further understand why the introduction of PPGDGE improves device stability, the possible reaction pathway of PPGDGE in the PPN solution was analyzed, as shown in Figure 4a. In stage 1, under acidic conditions,[27] the two epoxy groups in PPGDGE are first protonated to form oxonium ions. Subsequently, the sulfonic acid groups in PSS attack the carbon atoms of the epoxy groups in stage 2.[18] After deprotonation in stage 3, new C−O bonds are formed between the O atoms of the sulfonic acid groups and the C atoms of the epoxy groups. Due to the presence of two epoxy groups in PPGDGE molecules, PPGDGE can form linkages with the sulfonic acid groups of PSS during the reaction process, thereby constructing a cross-linked network structure in stage 3. The presence of this cross-linked structure can restrain the hygroscopic behavior of the film, thereby reducing the internal hygroscopicity of the PPN film and improving the device stability. Meanwhile, the water contact angle of the PPN-GDGE film was also measured, as shown in Figure S9. The water contact angle was 100.81°, indicating that the introduction of PPGDGE did not destroy the surface hydrophobicity of the film.

To verify the occurrence of this reaction, the FTIR spectra of PPGDGE, PPN film, and PPN-GDGE films were analyzed, as shown in Figure 4b,c. Peaks at 838 and 907 cm^{-1} were the vibrations of the epoxy group, and the vibration of C−O−C was found at 1091 cm^{-1}.[28,29] The peaks at 2870 and 2972 cm^{-1} were methylene and methyl.[30,31] As shown in Figure 4c, compared with the PPN film, the characteristic peaks associated with the epoxy groups disappear in the PPN-GDGE film, indicating that the epoxy groups underwent reaction. For the PPN film, the peaks at 862 and 998 cm^{-1} are assigned to the C−S bonds of the thiophene ring in PEDOT,[32] while the peak at 1048 cm^{-1} corresponds to SO_3^-.[33] It was found that the SO_3^- peak of PPN-GDGE shifts to 1044 cm^{-1}. This shift toward a lower wavenumber further indicates that the sulfonic acid groups participated in this reaction. Considering that this reaction generates new C−O bonds, the XPS spectra of C 1s of the two films were further analyzed, as shown in Figure 4d,e. The peak at 291.8 eV is assigned to the CF_2 of Nafion. In addition, the area ratio of the C−O peak to the C—C/C═C peak increased from 0.53 in the PPN film to 0.75 in the PPN-GDGE film, indicating an increase in the proportion of C−O bonds in the film. This further confirmed the occurrence of the reaction.

To further verify the reduced internal hygroscopicity of the film, Raman spectra of the pristine PEDOT:PSS, PPN, and PPN-GDGE films, as well as of the corresponding films after storage in air for 500 h, were analyzed, as shown in Figure 5a−c. The characteristic PEDOT peak at 1436 cm^{-1} in the PEDOT:PSS film blue-shifts to 1441 cm^{-1} after 500 h. During the stability monitoring of PEDOT:PSS/Si hybrid solar cells, this blue-shift is usually associated with the hygroscopicity of PEDOT:PSS and can induce conformational changes in PEDOT, thereby damaging the PCE of the device.[13,16] The Raman spectra of the PPN film are shown in Figure 5b. A blue-shift of the same characteristic peak is also observed, but the extent of the shift is smaller than that of the PEDOT:PSS film because of the surface hydrophobicity of the film. For the PPN-GDGE film, the peak position remains almost unchanged before and after 500 h of storage, as shown in Figure 5c. This indicates that the cross-linked network indeed reduced the internal hygroscopicity of the film.

In addition, humid environments can accelerate the formation of the SiO_x layer on the Si surface,[34] which is detrimental to the long-term stability of Si hybrid solar cells.[16,18] In Figure 5d, the HF-etched Si surface exhibits the lowest SiO_x peak intensity at 102.2 eV, whereas the Si surface after the removal of the PEDOT:PSS film shows the highest SiO_x peak intensity. The SiO_x peak intensity for the Si surface after the removal of the PPN film is close to that of PEDOT:PSS, indicating that although the film surface is hydrophobic, the film still possesses a certain degree of internal hygroscopicity. The SiO_x peak intensity after the removal of the PPN-GDGE film is lower than those of both PEDOT:PSS and PPN, indicating that the internal hygroscopic behavior of the PPN film was restrained. As a result, it can effectively retard the growth of SiO_x, which is beneficial for maintaining the stability of the device.

In summary, a PEDOT derivative film with surface hydrophobicity and reduced internal hygroscopicity was designed based on the dual-sulfonated polymer PSS and Nafion. Different contact sequences among EDOT, PSS, and Nafion led to different electric conductivities of the PPN, PNP, and PPP films, which were 36.51, 31.41, and 24.07 S/cm, respectively. The surface hydrophobicity of the film was mainly affected by EG introduction rather than the contact sequence, and all EG-treated films exhibited water contact angles above 100°. Compared with PPN, the introduction of PPGDGE restrained the internal hygroscopic behavior of the film and reduced its hygroscopicity. The Si hybrid solar cells based on this film exhibited a PCE of 7.59%. After 432 h of storage in air, the devices still retained 78% of their initial PCE, significantly higher than the 62% of the uncross-linked device and the 57% of conventional PEDOT:PSS. It is expected to be further applied in the fabrication of other optoelectronic devices, such as all-perovskite tandem solar cells and organic solar cells.

■ ASSOCIATED CONTENT

Supporting Information

The Supporting Information is available free of charge at https://pubs.acs.org/doi/10.1021/acs.jpclett.6c00980.

Preparation process of the PEDOT derivative; XPS spectra, electric conductivity, and thickness of different films; dark $I-V$ curves of different films; structural evolution, surface morphology, and water contact angle of films with different contact sequences; $J-V$ curves and performance parameters of PEDOT derivative/Si hybrid solar cells; EQE spectra of PEDOT derivative/Si and PEDOT:PSS/Si hybrid solar cells; and experimental details (PDF)

■ AUTHOR INFORMATION

Corresponding Author

Meicheng Li − *State Key Laboratory of Alternate Electrical Power System with Renewable Energy Sources, School of New Energy, North China Electric Power University, Beijing*

https://doi.org/10.1021/acs.jpclett.6c00980
J. Phys. Chem. Lett. 2026, 17, 5880−5888

*102206, China; orcid.org/0000-0002-0731-741X; Email: mcli@ncepu.edu.cn

Authors

Qi Geng − *State Key Laboratory of Alternate Electrical Power System with Renewable Energy Sources, School of New Energy, North China Electric Power University, Beijing 102206, China*

Wangbo Liu − *State Key Laboratory of Alternate Electrical Power System with Renewable Energy Sources, School of New Energy, North China Electric Power University, Beijing 102206, China*

Yuzhou Liu − *State Key Laboratory of Alternate Electrical Power System with Renewable Energy Sources, School of New Energy, North China Electric Power University, Beijing 102206, China*

Zhe Wang − *State Key Laboratory of Alternate Electrical Power System with Renewable Energy Sources, School of New Energy, North China Electric Power University, Beijing 102206, China*

Zhongliang Gao − *School of Electrical and Electronic Engineering, Shandong University of Technology, Zibo 255000, China; orcid.org/0000-0001-8211-9985*

Xin Sun − *State Key Laboratory of Alternate Electrical Power System with Renewable Energy Sources, School of New Energy, North China Electric Power University, Beijing 102206, China*

Yingfeng Li − *State Key Laboratory of Alternate Electrical Power System with Renewable Energy Sources, School of New Energy, North China Electric Power University, Beijing 102206, China*

Xiaojun Lv − *State Key Laboratory of Alternate Electrical Power System with Renewable Energy Sources, School of New Energy, North China Electric Power University, Beijing 102206, China*

Complete contact information is available at: https://pubs.acs.org/10.1021/acs.jpclett.6c00980

Author Contributions

The manuscript was written through contributions of all authors. All authors have given approval to the final version of the manuscript.

Notes

The authors declare no competing financial interest.

■ ACKNOWLEDGMENTS

This work is supported partially by the National Natural Science Foundation of China (Grant nos. 52232008, 52302250, and 62304125), Beijing Natural Science Foundation (2222076), Hebei Natural Science Foundation (B2024502013), the project of China Three Gorges Corporation named key technologies of intelligent joint regulation and operation with grid connected friendly in power station group of wind, solar photovoltaic and energy storage (WWKY-2021-0173), Huaneng Group Headquarters Science and Technology Project (HNKJ20-H88), the Fundamental Research Funds for the Central Universities (2025MS046), and the NCEPU "Double First-Class" Program.

■ REFERENCES

(1) Li, J.; Fan, L.; Bai, J.; Zhang, L.; Tian, J. Triton-X Engineered Hole-Injection Layer Enabled Efficient Flexible Quantum Dot Light-Emitting Diodes. *Adv. Opt Mater.* **2025**, *13* (30), No. e01635.

(2) Lai, H.; Zhu, J.; Kuo, R.-T.; Aeberhard, U.; Lin, Z.-H.; Mrkyvkova, N.; Luo, J.; Siegrist, S.; Wechsler, P.; Shih, C.-J.; Siffalovic, P.; Chen, C.; Tiwari, A. N.; Lin, T.-Y.; Zhao, D.; Fu, F. Tailored PEDOT:PSS phase segregation for high-efficiency flexible all-perovskite tandem solar cells and mini-modules. *Nat. Commun.* **2025**, *16* (1), 11468.

(3) Zhu, J.; Xu, Y.; Luo, Y.; Luo, J.; He, R.; Wang, C.; Wang, Y.; Wei, K.; Yi, Z.; Gao, Z.; Wang, J.; You, J.; Zhang, Z.; Lai, H.; Ren, S.; Liu, X.; Xiao, C.; Chen, C.; Zhang, J.; Fu, F.; Zhao, D. Custom-tailored hole transport layer using oxalic acid for high-quality tin-lead perovskites and efficient all-perovskite tandems. *Sci. Adv.* **2024**, *10* (16), No. eadl2063.

(4) Luo, Z.; Yang, C.; Chen, X.; Ma, W.; Li, S.; Fu, K. Improving open-circuit voltage and short-circuit current of high-efficiency silicon-based planar heterojunction solar cells by combining V_2O_5 with PEDOT:PSS. *J. Materiomics* **2023**, *9* (3), 438−446.

(5) Yu, L.-M.; Man, J.-X.; Chen, T.; Luo, D.; Wang, J.; Yang, H.; Zhao, Y.-B.; Wang, H.; Yang, Y.; Lu, Z.-H. Colorful conducting polymers for vivid solar panels. *Nano Energy* **2021**, *85*, No. 105937.

(6) Srivastava, A.; Sharma, D.; Kumari, P.; Dutta, M.; Srivastava, S. K. Highly Efficient PEDOT:PSS/Silicon Hybrid Solar Cells via Effective Surface Microengineering of Low-Cost Solar-Grade Silicon Wafers. *ACS Appl. Energy Mater.* **2021**, *4* (4), 4181−4198.

(7) Zielke, D.; Gogolin, R.; Halbich, M.-U.; Marquardt, C.; Lövenich, W.; Sauer, R.; Schmidt, J. Large-Area PEDOT:PSS/c-Si Heterojunction Solar Cells With Screen-Printed Metal Contacts. *Sol. RRL* **2018**, *2* (3), No. 1700191.

(8) Yoon, S.-S.; Khang, D.-Y. High Efficiency (>17%) Si-Organic Hybrid Solar Cells by Simultaneous Structural, Electrical, and Interfacial Engineering via Low-Temperature Processes. *Adv. Energy Mater.* **2018**, *8* (9), No. 1702655.

(9) Zhang, X.; Yang, D.; Yang, Z.; Guo, X.; Liu, B.; Ren, X.; Liu, S. Improved PEDOT:PSS/c-Si hybrid solar cell using inverted structure and effective passivation. *Sci. Rep.* **2016**, *6* (1), 35091.

(10) Wan, L.; Zhang, C.; Ge, K.; Yang, X.; Li, F.; Yan, W.; Xu, Z.; Yang, L.; Xu, Y.; Song, D.; Chen, J. Conductive Hole-Selective Passivating Contacts for Crystalline Silicon Solar Cells. *Adv. Energy Mater.* **2020**, *10* (16), No. 1903851.

(11) Liu, H.; Liu, Q.; Liu, J.; Zhao, Y.; Yu, Y.; An, Y.; Wei, G.; Li, Y.; Fu, Y.; Li, J.; He, D. Effects of different interface on the stability of hybrid heterojunction solar cells. *Sol. Energy Mater. Sol. Cells* **2024**, *264*, No. 112624.

(12) Bießmann, L.; Kreuzer, L. P.; Widmann, T.; Hohn, N.; Moulin, J.-F.; Müller-Buschbaum, P. Monitoring the Swelling Behavior of PEDOT:PSS Electrodes under High Humidity Conditions. *ACS Appl. Mater. Interfaces* **2018**, *10* (11), 9865−9872.

(13) Jiang, L.; Zhou, Z.; Zhang, G.; Li, C.; Feng, Q.; Wei, Q.; Li, J.; Wu, H.; Shi, Y.; Wang, J.; Yang, Y. Waterborne Acrylic Resin-Modified PEDOT:PSS as a Hole-Transporting Layer for Silicon/Organic Solar Cells with Improved Efficiency and Stability. *ACS Appl. Energy Mater.* **2024**, *7* (9), 3927−3936.

(14) Shen, R.; Sun, Z.; Zhou, Y.; Shi, Y.; Shang, J.; Chen, H.; Zhou, Y.; Liu, F. Organic/silicon nanowires hybrid solar cells using isobutyltriethoxysilane incorporated poly(3,4-ethylenedioxythiophene):poly (styrenesulfonate) as hole transport layer. *Prog. Photovolt.* **2022**, *30* (6), 661−669.

(15) He, J.; Gao, P.; Ling, Z.; Ding, L.; Yang, Z.; Ye, J.; Cui, Y. High-Efficiency Silicon/Organic Heterojunction Solar Cells with Improved Junction Quality and Interface Passivation. *ACS Nano* **2016**, *10* (12), 11525−11531.

(16) He, J.; Gao, P.; Yang, Z.; Yu, J.; Yu, W.; Zhang, Y.; Sheng, J.; Ye, J.; Amine, J. C.; Cui, Y. Silicon/Organic Hybrid Solar Cells with 16.2% Efficiency and Improved Stability by Formation of Conformal Heterojunction Coating and Moisture-Resistant Capping Layer. *Adv. Mater.* **2017**, *29* (15), No. 1606321.

(17) Lv, M.; Wang, Z.; Jiao, C.; Zhao, Y.; Jin, L.; Fu, Y.; Liu, Q.; He, D. High-Efficiency Si/PEDOT:PSS Hybrid Heterojunction Solar Cells Using Solution-Processed Graphene Oxide as an Antireflection and Inversion-Induced Layer. *ACS Appl. Energy Mater.* **2021**, *4* (11), 13279−13287.
(18) Liu, Y.; Geng, Q.; Wang, Z.; Liu, Z.; Gao, Z.; Sun, X.; Li, Y.; Li, M. Through Ring-Opening Reactions To Weaken the Hygroscopicity of PEDOT:PSS Films with Improved Stability of Silicon Hybrid Solar Cells. *ACS Appl. Mater. Interfaces* **2025**, *17* (45), 62022−62031.
(19) Carli, S.; Di Lauro, M.; Bianchi, M.; Murgia, M.; De Salvo, A.; Prato, M.; Fadiga, L.; Biscarini, F. Water-Based PEDOT:Nafion Dispersion for Organic Bioelectronics. *ACS Appl. Mater. Interfaces* **2020**, *12* (26), 29807−29817.
(20) Jiang, Y.; Dong, X.; Sun, L.; Liu, T.; Qin, F.; Xie, C.; Jiang, P.; Hu, L.; Lu, X.; Zhou, X.; Meng, W.; Li, N.; Brabec, C. J.; Zhou, Y. An alcohol-dispersed conducting polymer complex for fully printable organic solar cells with improved stability. *Nat. Energy* **2022**, *7* (4), 352−359.
(21) Geng, Q.; Liu, Z.; Liu, Y.; Wang, Z.; Gao, Z.; Sun, X.; Li, Y.; Chen, L.; Lv, X.; Li, M. Air-stable silicon hybrid solar cells constructed via hydrophobic polymer film. *J. Materiomics* **2025**, *11* (3), No. 100935.
(22) Zhou, X.; Fang, S.; Hu, Y.; Du, X.; Ding, H.; Chai, R.; Han, J.; Xie, J.; Gu, Z. Photoinduced double hydrogen-atom transfer for polymerization and 3D printing of conductive polymer. *Nat. Synth.* **2024**, *3* (9), 1145−1157.
(23) Sun, Z.; He, Y.; Xiong, B.; Chen, S.; Li, M.; Zhou, Y.; Zheng, Y.; Sun, K.; Yang, C. Performance-Enhancing Approaches for PEDOT:PSS-Si Hybrid Solar Cells. *Angew. Chem., Int. Ed.* **2021**, *60* (10), 5036−5055.
(24) Berlinger, S. A.; McCloskey, B. D.; Weber, A. Z. Inherent Acidity of Perfluorosulfonic Acid Ionomer Dispersions and Implications for Ink Aggregation. *J. Phys. Chem. B* **2018**, *122* (31), 7790−7796.
(25) Kuo, A.-T.; Urata, S.; Nakabayashi, K.; Watabe, H.; Honmura, S. Coarse-Grained Molecular Dynamics Simulation of Perfluorosulfonic Acid Polymer in Water−Ethanol Mixtures. *Macromolecules* **2021**, *54* (2), 609−620.
(26) Srivastav, H.; Weber, A. Z.; Radke, C. J. Colloidal Stability of PFSA-Ionomer Dispersions Part II: Determination of Suspension pH Using Single-Ion Potential Energies. *Langmuir* **2024**, *40* (13), 6666−6674.
(27) Abdul Jaleel, S. A.; Kim, T.; Baik, S. Covalently Functionalized Leakage-Free Healable Phase-Change Interface Materials with Extraordinary High-Thermal Conductivity and Low-Thermal Resistance. *Adv. Mater.* **2023**, *35* (30), No. 2300956.
(28) Castillejos, S.; Cerna, J.; Meléndez, F.; Castro, M. E.; Aguilar, R.; Márquez-Beltrán, C.; González, M. Bulk Modification of Poly(lactide) (PLA) via Copolymerization with Poly(propylene glycol) Diglycidylether (PPGDGE). *Polymers* **2018**, *10* (11), 1184.
(29) Zhuo, H.; He, Z.; Liu, J.; Ma, G.; Ren, Z.; Zeng, Y.; Chen, S. Bulk Polymerization of Thermoplastic Shape Memory Epoxy Polymer for Recycling Applications. *Polymers* **2023**, *15* (4), 809.
(30) Huang, X.; Wang, L.; Lai, Y.; Li, L.; Jiang, X.; Zhang, X. Fabrication of a nonionic self-emulsifiable waterborne epoxy curing agent with high cure properties. *J. Coat. Technol. Res.* **2021**, *18* (2), 549−558.
(31) Chen, X.; Liu, F. Synthesis and Phase Behavior of a Linear Amphiphilic Multiblock Copolymer. *ACS Omega* **2022**, *7* (23), 19319−19327.
(32) Han, M. G.; Foulger, S. H. Crystalline Colloidal Arrays Composed of Poly(3,4-ethylenedioxythiophene)-Coated Polystyrene Particles with a Stop Band in the Visible Regime. *Adv. Mater.* **2004**, *16* (3), 231−234.
(33) Nakajima, K.; Hara, M. Amorphous Carbon with SO_3H Groups as a Solid Brønsted Acid Catalyst. *ACS Catal.* **2012**, *2* (7), 1296−1304.
(34) Jäckle, S.; Liebhaber, M.; Niederhausen, J.; Büchele, M.; Félix, R.; Wilks, R. G.; Bär, M.; Lips, K.; Christiansen, S. Unveiling the Hybrid n-Si/PEDOT:PSS Interface. *ACS Appl. Mater. Interfaces* **2016**, *8* (13), 8841−8848.

https://doi.org/10.1021/acs.jpclett.6c00980
J. Phys. Chem. Lett. 2026, 17, 5880−5888